Physics Letters A 381 (2017) 2107–2111

Contents lists available at ScienceDirect

Physics Letters A

www.elsevier.com/locate/pla

Discussion

Electronic transport properties in [n]cycloparaphenylenes molecular devices

Lizhi Hu [a,b], Yandong Guo [a,b,*], Xiaohong Yan [a,b,c,*], Hongli Zeng [b,d], Jie Zhou [a,b]

[a] College of Electronic Science and Engineering, Nanjing University of Posts and Telecommunications, Nanjing 210046, China
[b] Key Laboratory of Radio Frequency and Micro-Nano Electronics of Jiangsu Province, Nanjing 210023, China
[c] College of Science, Nanjing University of Aeronautics and Astronautics, Nanjing 210016, China
[d] College of Natural Science, Nanjing University of Posts and Telecommunications, Nanjing 210046, China

ARTICLE INFO

Article history:
Received 29 November 2016
Received in revised form 19 March 2017
Accepted 24 April 2017
Available online 29 April 2017
Communicated by R. Wu

Keywords:
Cycloparaphenylenes
Electronic transport
Negative differential resistance
Density-functional theory
Nonequilibrium Green's function

ABSTRACT

The electronic transport of [n]cycloparaphenylenes ([n]CPPs) is investigated based on nonequilibrium Green's function formalism in combination with the density-functional theory. Negative differential resistance (NDR) phenomenon is observed. Further analysis shows that the reduction of the transmission peak induced by the bias changing near Fermi energy results in the NDR effect. Replacing the electrode (from carbon chain to Au electrode), doping with N atom and changing the size of the nanohoop (n = 5, 6, 8, 10) have also been studied and the NDR still exists, suggesting the NDR behavior is the intrinsic feature of such [n]CPPs systems, which would be quite useful in future nanoelectronic devices.

1. Introduction

In recent years, microfabrication and selfassembly techniques [1] have achieved much progress, which made it possible to design molecular devices, such as lithographically fabricated nanoelectrodes and mechanically controllable break junctions [2–5]. The electronic transport properties in molecular devices have been paid a lot of attention because many interesting phenomena have been found in these devices, such as negative differential resistance (NDR) [6–11], highly nonlinear *I–V* relationship [12], and electrical switching [13,14] etc. Because of the wide applications e.g., logic, memory, amplification, NDR attracts lots of attention.

Recently, the synthesis of [n]cycloparaphenylenes ([n]CPPs) has attracted ample interest due to their unique geometry [15–17]. In structure, [n]CPP molecules are made up of several fully conjugated bent benzenes. For example, [6]CPP is constructed by 6 benzenes, which have been synthesized by Xia et al. [18] and Kayahara et al. [19] in different ways. [6]CPP is the second smallest cycloparaphenylene to be synthesized, and [5]CPP is the smallest. As is well known, the molecular system structured with benzenes has been discovered to exhibit many fantastic electronic transport properties and has been designed for various devices such as logic gates, data transfer and tunnel-orientation rotator [20]. As a similar structure, [n]CPPs may have great potential application in future nano-devices. Although much attention has been paid to the synthesis of [n]CPPs, few of them focus on the electronic transport of these molecules. In this paper, we investigate the electronic transport properties of them.

[n]CPPs have various structure sizes. To make a balance between the calculation and the accuracy, we take the system of n = 6 as an example to carry out our research. Otherwise, we study the electronic and transport properties of nanohoops with different size, such as n = 5, 8, and 10. We take [6]CPP as an example to study the electronic transport with the method of density functional theory (DFT) and nonequilibrium Green's function (NEGF). It is interestingly found that NDR phenomenon is observed. The influence of the molecule-electrode contact geometry on the NDR is discussed. Considering the practical application, we replace the carbon chain electrodes with Au electrodes and the NDR phenomenon still exists. Furthermore, We study the transport properties of [5]CPP, [6]CPP, [8]CPP, [10]CPP and [6]CPP doped with N atom and all the *I–V* curves we obtained show NDR behavior. These results suggest the NDR behavior is the intrinsic feature of the [n]CPP device.

* Corresponding authors.
E-mail addresses: yandongguo@njupt.edu.cn (Y.D. Guo), xhyan@njupt.edu.cn (X.H. Yan).

http://dx.doi.org/10.1016/j.physleta.2017.04.035
0375-9601/

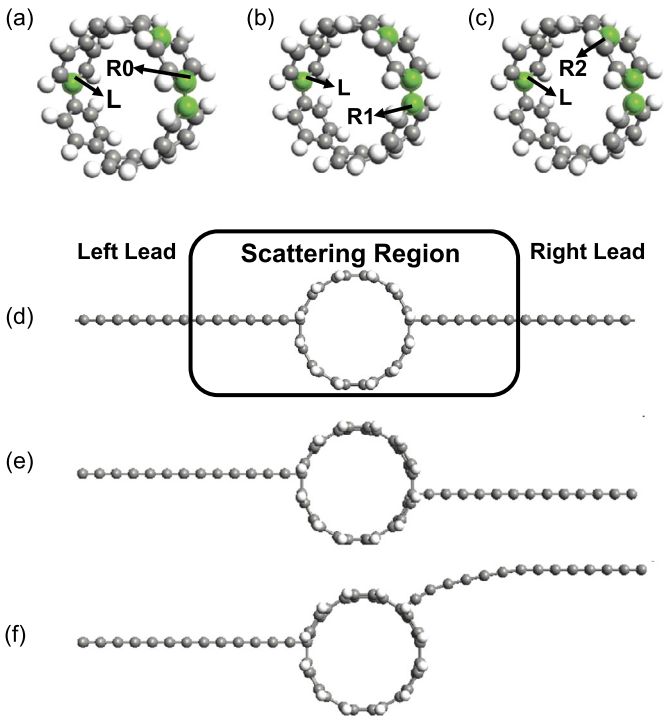

Fig. 1. (Color online.) (a)–(c) the profiles of the [6]CPP. The L contacts the left lead and the R0, R1, and R2 contact the right lead, respectively. (d)–(f) Geometry of the three C-[6]CPP-C systems, the carbon atomic chain electrodes are attached to two carbon atoms on either side of the structure with a fixed optimal separation of 1.27 Å.

2. Computational method

[6]CPP possesses an architecture of six fully conjugated bent benzenes linked in the para position to form a nanohoop, as shown in Fig. 1(a). It can be seen as being cut from a [6, 6] armchair carbon nanotube (CNT) [18]. The molecule is saturated with H atoms around the benzenes to eliminate the dangling bonds. We use the carbon linear atomic chains as electrodes to get rid of complications which may arise from electrode-molecule interactions [21]. These chains are good electrode candidates because of their metallicity and their atomically sharp tips. The bond length in the linear chain is set to be 1.27 Å [22]. We carry out our calculations with the Atomistix Toolkit package [23,24] which is based on the combination of DFT and NEGF. We use the mesh cut-off energy of 150 Ry, and $1 \times 1 \times 100$ k-point mesh in the Monkhorst–Pack scheme. The Perdew–Burke–Eenzerhof formulation of the generalized gradient approximation to the exchange-correlation function is used. The double-zeta polarized basis set of local numerical orbitals is employed in all our calculations. The supercell with sufficient vacuum spaces (more than 10 Å) is chosen to prevent the interactions with adjacent images. To mimic the actual situation, the positions of all atoms in the nanohoop are fully relaxed before the transport calculations and the maximal forces are set to be 0.02 eV/Å.

3. Results and discussions

As for the contact geometry, we in this paper consider three cases, which are illustrated in Fig. 1(a)–(c). Figure 1(a)–(c) show the molecular part of the whole system. The left lead is always connected to the same carbon atom (L) of the molecule and the right lead is coupled to the different carbon atoms (R0–R2) for the three cases, respectively. After contacting electrodes, the whole [6]CPP molecular transport system is illustrated schematically in Fig. 1(d)–(f). As we can see in Fig. 1(d), the system is divided into

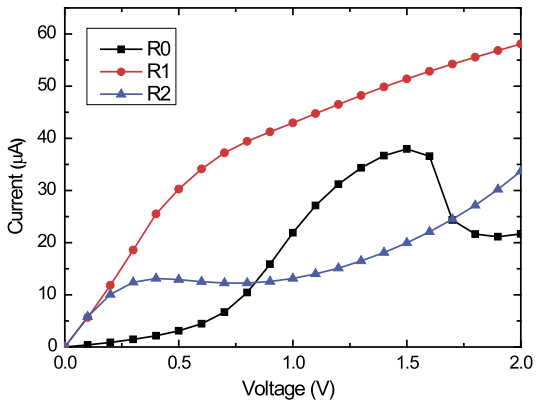

Fig. 2. (Color online.) Calculated current as a function of the applied bias for the C-[6]CPP-C system with different positions of the right C lead, respectively.

three parts: the left and right electrodes and the central scattering region and the others are the same. Actually, a portion of the semi-infinite electrodes are included in the central scattering region. The linear C atomic chains are modeled as the semi-infinite in our system.

In Fig. 2, we describe the current as a function of the applied bias voltage from 0 to 2.0 V for R0–R2 and we can find that all the three systems show metallic transport behavior. From the figure, one finds that the current of R1 is remarkably larger than that of R0 and R2 for the whole bias range from 0 to 2.0 V. This means that the contact geometries of R0 and R2 weaken the electronic transport and lead to smaller current. When the bias takes a value between 1.5 and 1.9 V, the current of R0 decreases obviously with the increase of the bias, which shows NDR behavior in this bias range. However, the NDR behavior does not occur in the other two contact-site cases. Therefore, it can be concluded that the contact site is crucial for the current-voltage characteristics and we can tune the system by changing the sites connected to the electrodes.

We calculate the total energies of the three contact-site cases and the results are −10099.425, −10094.259, −10092.165 eV for R0, R1 and R2, respectively. From the data we can see that R0 system possesses the lowest total energy, which is the most stable geometry. It should be noted that, the R0 system shows the NDR phenomenon which is the result we expect.

As we all know, the current of the system is of dependence on the transmission coefficient directly. For the sake of the explanation of the NDR phenomenon seen in Fig. 2, we plot the transmission spectra and the corresponding projection of the density of states (PDOS) for the I–V curve of the R0 system at bias voltages of 1.5, 1.9, and 2.0 V, respectively, shown in Fig. 3(a1)–(a3). The PDOS could give us the information of the molecular orbitals which are associated with the eigenstates of the system, line broadening, and the energy shift. By integrating the transmission coefficient into the bias window, we can get the current of the system. When the bias is 1.5 V, Fig. 3(a1) shows that there are two strong and wide transmission peaks originating from the peaks in the PDOS that lies in bias window, which attributes to a large current. Thus we can see that there is a strong coupling between the carbon electrode and the molecule, which leads to the electronic transport in the [6]CPP system. When the bias is set between 1.5 and 1.9 V, although the bias window increases with the bias voltage, the total integral area gets smaller. As a result, the current decreases and the NDR appears. However, in Fig. 3(a2), the PDOS is the same as that shown in Fig. 3(a1), there is only a transmission peak located in the bias window compared with Fig. 3(a1) and the peak is smaller than that. We will give a further explanation about the difference between them later. From Fig. 3(a3), one can find that when the bias voltage is further increased, more integral area gets

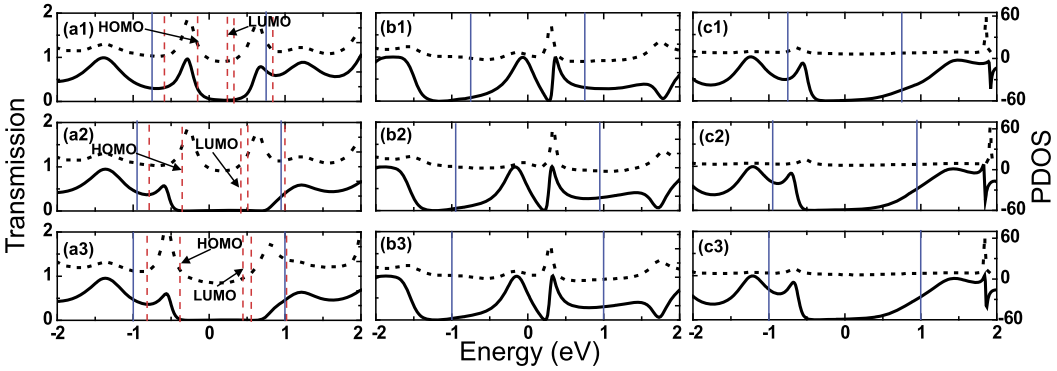

Fig. 3. (Color online.) Describe the transmission coefficient (solid curves) and the corresponding projection of the density of states (PDOS) (dotted curves) for the R0, R1, and R2 system under bias voltages of 1.5, 1.9, and 2.0 V, respectively. (a1)–(a3) correspond to the R0 system under bias voltages of 1.5, 1.9, and 2.0 V; (b1)–(b3) correspond to the R1 system under bias voltages of 1.5, 1.9, and 2.0 V; (c1)–(c3) correspond to the R2 system under bias voltages of 1.5, 1.9, and 2.0 V. The Fermi level has been set to E_F=0 and the solid blue lines indicate the bias window.

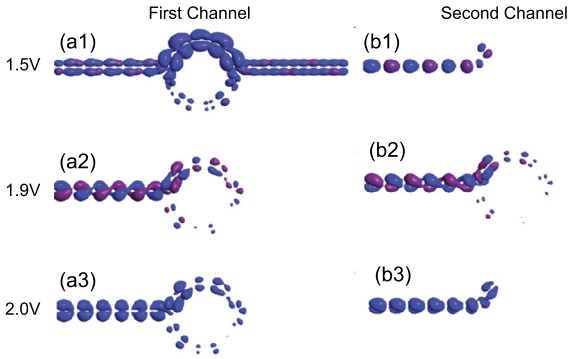

Fig. 4. (Color online.) The transmission eigenchannels at E = −0.27 eV under different bias voltages of R0 system. (a1)–(a3) correspond to the first channel under the bias voltages of 1.5, 1.9 and 2.0 V; (b1)–(b3) correspond to the second channel under the bias voltages of 1.5, 1.9 and 2.0 V.

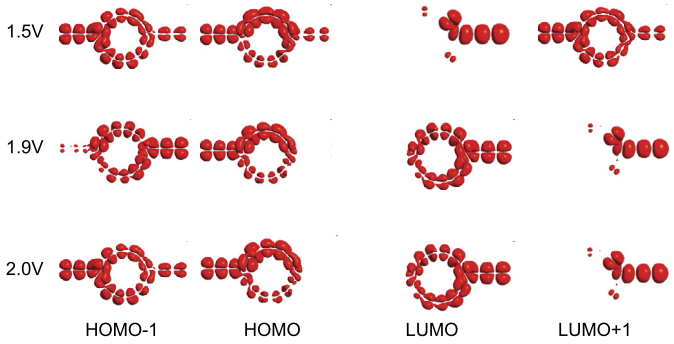

Fig. 5. (Color online.) The molecular projected self-consistent Hamiltonian (MPSH) of R0 system for the four frontier molecular orbitals under 1.5, 1.9 and 2.0 V, respectively.

Table 1
Transmission eigenvalues of eigenchannels at E = −0.27 eV in Fig. 4.

	First channel	Second channel
1.5 V	0.9361	0.0001
1.9 V	0.0004	0.0001
2.0 V	0.0006	0.0002

into the bias window before the current increases again and the NDR disappears, where the transmission spectrum almost remains unchanged. From Fig. 3(b1)–(b3), we can see that the transmission spectra are almost the same at different bias voltages and the current increases all the time in the certain bias range due to the increasing bias integral window. In Fig. 3(c1)–(c3), the same variation trend can be found in Fig. 3b. Therefore, one can only find the obvious NDR behavior in the R0 system, while the currents of the R1 and R2 system increase generally. These results show that different contact geometries can affect the electronic transport and some of them show the NDR phenomenon, while the others do not.

To understand the origin of the peaks which are suppressed in transmission curves in Fig. 3(a2), we calculate the transmission eigenvalues and plot corresponding eigenchannels, shown in Table 1 and Fig. 4, respectively. The results show that there are two eigenchannels dominating the electronic transport. In the Fig. 3(a1), there are two strong and wide transmission peaks at E = −0.27 and 0.63 eV originating from the peaks in the PDOS that lies in bias window, which attribute to a large current. Apparently, for the bias of 1.5 V, the first transmission eigenchannel at −0.27 eV is delocalized throughout the two-probe system, as shown in Fig. 4(a1) which corresponds to the transmission eigenvalue of 0.9361 in Table 1. This channel is almost totally opened. While, for the bias of 1.9 V, the channels become localized for both the first and second ones, see Fig. 4(a2) and (b2). As a result, this leads to a smaller current although the bias increases. For 2.0 V, both transmission eigenchannels remain localized as shown in Fig. 4(a3) and (b3), but the current increases a little due to the larger integral window. Besides, we also calculate the transmission eigenvalues and plot the eigenchannels at E = 0.63 eV for the bias V = 1.5, 1.9, and 2.0 V and draw the same conclusion as that at E = −0.27 eV (not shown). As a consequence, the NDR emerges. To confirm the mechanism, we performed the analysis of projected self-consistent Hamiltonian (MPSH).

For R0 configuration, we calculate and plot the molecular MPSH of the four frontier molecular orbitals HOMO-1, HOMO (highest occupied molecular orbital), LUMO (lowest unoccupied molecular orbital) and LUMO+1 at 1.5, 1.9 and 2.0 V, which corresponds to those in Fig. 3(a1)–(a3). The eigenstates of MPSH can be considered as molecular orbitals renormalized by the molecule-electrode interaction. From Fig. 5, one can clearly see that the HOMO under 1.5 V is delocalized throughout the two-probe system, which contributes to a larger transmission coefficient near the Fermi level in Fig. 3(a1). However, the HOMO at 1.9 and 2.0 V become more localized compared with that at 1.5 V, which leads to a small transmission coefficient. We can analyze the LUMO+1 state in the same way and arrive at the same conclusion. In brief, the variation trend of MPSH coincides with those of transmission eigenchannels.

However, in experimental and practical applications, the metal electrode is more commonly used. In order to study the electronic transport properties of the [n]CPPs with the metal electrodes, we choose the nanostructure of Au as the representative to build a

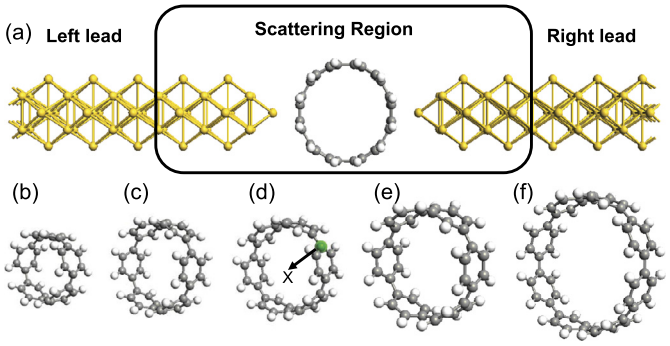

Fig. 6. (Color online.) (a) Geometry of the Au-[6]CPP-Au system. (b)–(f) the profile of [5]CPP, [6]CPP, [6]CPP doped with X, [8]CPP and [10]CPP, respectively. X = N.

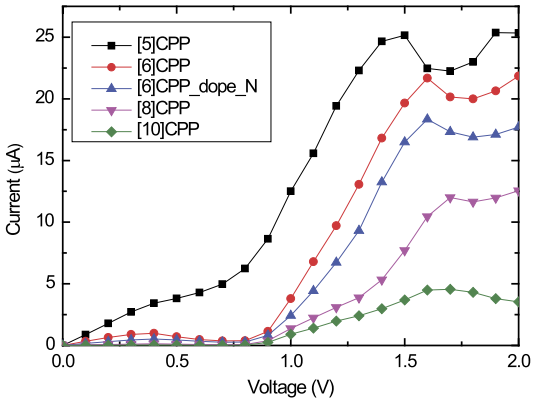

Fig. 7. (Color online.) Calculated current as a function of the applied bias for the Au-[n]CPP-Au system with different size of the nanohoop. n = 5, 6, 8, 10.

Au-[n]CPP-Au two-probe system. We still take the [6]CPP as an example to study. The setup of the whole system is shown in the Fig. 6(a). The [6]CPP is set between the left and right leads with a fixed distance which is optimized by minimizing the total energy. We set the distance between Au lead and the [6]CPP from 1.0 to 4.0 Å by step 0.1 Å and calculate the total energy for each step. Then we obtain a configuration with the lowest total energy and choose the corresponding distance to carry out our work. As we can see in Fig. 7, the *I–V* curve of the Au-[6]CPP-Au system shows a threshold bias voltage and the current goes to almost zero. For the [6]CPP system with carbon chain electrode in Fig. 2, there is not such an obvious gate voltage and a turn of the current also exists at 0.7 V. After the threshold bias voltage, the current is increasing obviously by the increasing bias voltage. However, the peak of the current in Fig. 7 is lower than the one for R0 system in Fig. 2, which may result from the change of electrode coupling. When the bias voltage is further increased to a certain range [1.6, 1.8] V, the current decreases and the NDR appears. The peak-to-valley ratios in Fig. 7 is 1.083, which is much smaller than the 1.795 for R0 system in Fig. 2. This indicates that the electrode can change the NDR behavior.

Besides, we also study the different sizes of the nanohoop in Fig. 6 and (b), (c), (e) and (f) represent the profile of [5]CPP, [6]CPP, [8]CPP and [10]CPP, respectively. Figure 7 shows the current of several systems as a function of the bias. From the figure, one can clearly find that all the four systems display NDR behavior at the certain bias voltage range, especially in the small nanohoop, such as [5]CPP or [6]CPP and all the curves except the [5]CPP show a threshold bias of about 0.9 V. This means that the NDR phenomenon is the robust in the [n]CPP system and [n]CPPs may have great potential application in future nano-devices.

As we know, doping other elements in carbon system can change the property of them. To check the influence of doping on the NDR, a systematic study is needed. Here, we only take a simple model to investigate, i.e., one carbon atom denoted by X in Fig. 6(d) is replaced by N atom. The corresponding *I-V* curve is shown in Fig. 7. Interestingly, the curve of the [6]CPP system doped with N atom has the same changing trend with the [6]CPP and the NDR behavior occurs at the same bias voltage. The NDR in such [n]CPP devices is also robust to doping.

4. Conclusion

In summary, by applying the first principles calculation, the electronic transport properties of [6]CPP are investigated and the NDR phenomenon is observed. The influence of the molecule-electrode contact geometry on the NDR is discussed. Further analysis shows that the PDOS and the MPSH features near Fermi energy result in the obvious NDR effect. Moreover, we also study the [5]CPP, [6]CPP, [6]CPP doped with N atom, [8]CPP and [10]CPP with Au electrodes and the NDR phenomenon still exists. Therefore, it can be clearly seen that the NDR behavior is the intrinsic feature of the [n]CPPs, which is quite beneficial in nanoelectronics.

Acknowledgements

This work is supported by the National Natural Science Foundation of China (NSFC11504178, NSFC11374162 and NSFC11247033), the Natural Science Foundation of Jiangsu Province (BK20150825 and TJ215009), the Scientific Research Foundation of Nanjing University of Posts and Telecommunications (NY214010 and NY-217013), and the Fundamental Research Funds for the Central Universities (NS2014173).

References

[1] R. Andres, T. Bein, M. Dorogi, S. Feng, J. Henderson, C. Kubiak, W. Mahoney, R. Osifchin, R. Reifenberger, "Coulomb staircase" at room temperature in a self-assembled molecular nanostructure, Science 272 (1996) 1323.
[2] X. Xiao, B. Xu, N. Tao, Measurement of single molecule conductance: benzenedithiol and benzenedimethanethiol, Nano Lett. 4 (2004) 267.
[3] S. Ghosh, H. Halimun, A. Mahapatro, J. Choi, S. Lodha, D. Janes, Device structure for electronic transport through individual molecules using nanoelectrodes, J. Appl. Phys. 87 (2005) 233509.
[4] T. Dadosh, Y. Gordin, R. Krahne, I. Khivrich, D. Mahalu, V. Frydman, J. Sperling, A. Yacoby, I. Bar-Joseph, Measurement of the conductance of single conjugated molecules, Nature 436 (2005) 677.
[5] M. Tsutsui, Y. Teramae, S. Kurokawa, A. Sakai, High-conductance states of single benzenedithiol molecules, J. Appl. Phys. 89 (2006) 163111.
[6] J. Chen, M. Reed, A. Rawlett, J. Tour, Large on-off ratios and negative differential resistance in a molecular electronic device, Science 286 (1999) 1550.
[7] J. Chen, W. Wang, M. Reed, A. Rawlett, D. Price, J. Tour, Room-temperature negative differential resistance in nanoscale molecular junctions, J. Appl. Phys. 77 (2000) 1224.
[8] M. Di Ventra, S. Pantelides, N. Lang, First-principles calculation of transport properties of a molecular device, Phys. Rev. Lett. 84 (2000) 979.
[9] W.Y. Kim, S.K. Kwon, K.S. Kim, Negative differential resistance of carbon nanotube electrodes with asymmetric coupling phenomena, Phys. Rev. B 76 (2007) 033415.
[10] M.Q. Long, K.Q. Chen, L. Wang, B.S. Zou, Z. Shuai, Negative differential resistance induced by intermolecular interaction in a bimolecular device, J. Appl. Phys. 91 (2007) 233512.
[11] L. Chen, Z. Hu, A. Zhao, B. Wang, Y. Luo, J. Yang, J. Hou, Mechanism for negative differential resistance in molecular electronic devices: local orbital symmetry matching, Phys. Rev. Lett. 99 (2007) 146803.
[12] Z. Crljen, A. Grigoriev, G. Wendin, K. Stokbro, Nonlinear conductance in molecular devices: molecular length dependence, Phys. Rev. B 71 (2005) 165316.
[13] D.I. Gittins, D. Bethell, D.J. Schiffrin, R.J. Nichols, A nanometre-scale electronic switch consisting of a metal cluster and redox-addressable groups, Nature 408 (2000) 67.
[14] I.C. Lekshmi, G. Berera, Y. Afsar, G.X. Miao, T. Nagahama, T. Santos, J.S. Moodera, Controlled synthesis characterization of Ag2SAg2S films with varied microstructures and its role as asymmetric barrier layer in trilayer junctions with dissimilar electrodes, J. Appl. Phys. 103 (2008) 093719.

[15] R. Jasti, C.R. Bertozzi, Progress and challenges for the bottom-up synthesis of carbon nanotubes with discrete chirality, Chem. Phys. Lett. 494 (2010) 1.
[16] E.S. Hirst, R. Jasti, Bending benzene: syntheses of [n] cycloparaphenylenes, Am. J. Org. Chem. 77 (2012) 10473.
[17] H. Omachi, Y. Segawa, K. Itami, Synthesis of cycloparaphenylenes and related carbon nanorings: a step toward the controlled synthesis of carbon nanotubes, Acc. Chem. Res. 45 (2012) 1378.
[18] J. Xia, R. Jasti, Synthesis, characterization, and crystal structure of [6] cycloparaphenylene, Angew. Chem., Int. Ed. Engl. 51 (2012) 2474.
[19] E. Kayahara, V.K. Patel, J. Xia, R. Jasti, S. Yamago, Selective and gram-scale synthesis of [6] cycloparaphenylene, Synlett 26 (2015) 1615.
[20] Y.D. Guo, X.H. Yan, Y. Xiao, Conformational change-induced switching behavior in pure-carbon systems, RSC Adv. 3 (2013) 16672.
[21] H. Sahin, R.T. Senger, First-principles calculations of spin-dependent conductance of graphene flakes, Phys. Rev. B 78 (2008) 205423.
[22] S. Tongay, R. Senger, S. Dag, S. Ciraci, Ab-initio electron transport calculations of carbon based string structures, Phys. Rev. Lett. 93 (2004) 136404.
[23] M. Brandbyge, J. Mozos, P. Ordejon, J. Taylor, K. Stokbro, Density-functional method for nonequilibrium electron transport, Phys. Rev. B 65 (2002) 165401.
[24] Quantumwise A/S, http://www.quantumwise.com/.